

Spin demons in d -wave altermagnets

Pieter M. Gunnink,^{1,*} Jairo Sinova,¹ and Alexander Mook¹

¹*Johannes Gutenberg University Mainz, Staudingerweg 7, Mainz 55128, Germany*

(Dated: March 25, 2025)

Demons are a type of plasmons, which consist of out-of-phase oscillations of electrons in different bands. Here, we show that d -wave altermagnets, a recently discovered new class of collinear magnetism, naturally realize a spin demon, which consists of out-of-phase movement of the two spin species. The spin demon lives outside of the particle-hole continuum of one of the spin species, and is therefore significantly underdamped, reaching quality factors of > 10 . We show that the spin demon carries a magnetic moment, which inherits the d -wave symmetry. Finally, we consider both three and two dimensional d -wave altermagnets, and show that spin demons exists in both.

Introduction. Altermagnets are a recently discovered class of collinear magnets, characterized by a by a sublattice transposing symmetry involving rotation or mirror operations [1, 2]. This results in anisotropically spin-split Fermi surfaces, which exhibit a d -wave (or higher even-parity) like order. These spin-split bands can give rise to unusual transport properties [2–4], piezomagnetism [5, 6], the generation of spin-splitter torque in MRAM geometries [7] and chiral split magnon bands [8, 9].

The existence of spin-split Fermi surfaces also opens up the possibility of an out-of-phase oscillation of the two spin densities, realizing a *demon*: an acoustic, electrically neutral type of plasmon, first proposed by Pines [10]. They are typically gapless, in contrast to the conventional in-phase charge plasmon in three dimensions, and have been predicted for numerous materials [10, 11], but are typically overdamped due to their overlap with the particle-hole continuum [12–15]. Recent works have however shown that with sufficient separation of the Fermi surfaces, the damping can be suppressed and well-defined quasiparticles are formed [14, 16].

In this work, we show that a d -wave altermagnetic metal can host a spin-polarized demon, which we dub a *spin demon*. In contrast to the conventional charge plasmon, the spin demon does not live completely outside of the particle-hole continuum, but only outside of the particle-hole continuum of one of the spin species. The spin demon is therefore not completely undamped, but can still reach quality factors of > 10 for realistic parameters, and is therefore well defined and long lived. We demonstrate the existence of the spin demon in both a three-dimensional (3D) and two-dimensional (2D) d -wave altermagnetic metal. We also establish that the spin demon inherits the d -wave symmetry of the altermagnetic order parameter, by demonstrating that it has a finite magnetic moment which changes sign as it is rotated through the altermagnetic spin-split plane.

The existence of the spin demon can be readily shown by calculating the spin-spin response function, $\text{Im}[\chi_{S_z S_z}(\mathbf{q}, \omega)]$, of an altermagnetic metal, which we show in the altermagnetic spin split plane in Fig. 1. The spin demon corresponds to the strongly peaked response in the spin-spin response function, $\text{Im}[\chi_{S_z S_z}(\mathbf{q}, \omega)]$, and follows the four-fold rotational symmetry of the d -wave altermagnet. In particular, it vanishes along the

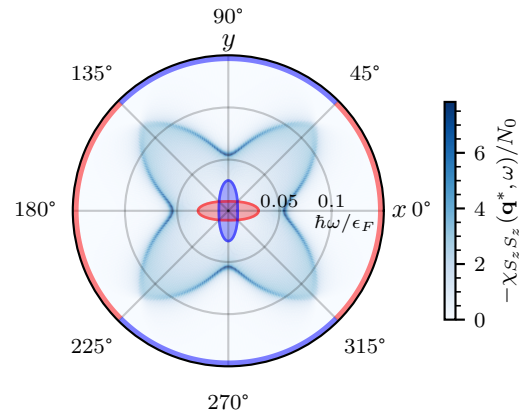


FIG. 1. The spin-density response function, $\text{Im}[\chi_{S_z S_z}(\mathbf{q}^*, \omega)]$, where $\mathbf{q}^* = q (\cos \theta, \sin \theta, 0)$, rotated in the altermagnetic spin split plane with a fixed $q = 0.05k_F$. The angle indicates θ and the radial axis the frequency ω . The colors on the ring indicate the projected spin species, with red (blue) spin up (down). The spin demon is the sharp resonance that follows the four-fold rotational symmetry of the d -wave altermagnet. The anisotropically spin-split Fermi surfaces are schematically shown at the origin.

high-symmetry axis, where the electron bands are degenerate. The spin demon corresponds to a longitudinal, out-of-phase, oscillation of the spin species, as we will show. In the four different quadrants of the altermagnetic spin split plane, the majority spin species in this out-of-phase oscillation changes, following the altermagnetic d -wave symmetry.

Method. We describe here the spin demon within the random phase approximation (RPA), where the spin-resolved response functions $\chi_{\sigma\sigma'}$ are given by [17]

$$\begin{pmatrix} \chi_{\uparrow\uparrow} & \chi_{\uparrow\downarrow} \\ \chi_{\downarrow\uparrow} & \chi_{\downarrow\downarrow} \end{pmatrix}^{-1} = \begin{pmatrix} \chi_{\uparrow}^{(0)} & 0 \\ 0 & \chi_{\downarrow}^{(0)} \end{pmatrix} - v_q \begin{pmatrix} 1 & 1 \\ 1 & 1 \end{pmatrix}. \quad (1)$$

Here, $\chi_{\sigma}^{(0)}$ is the non-interacting density-density response function for spin σ , and $v_q = e^2/\epsilon_0 q^2$ is the Fourier transform of the Coulomb interaction. We assume the altermagnet to be oriented such that the spin-splitting is maximal along the x , y -axis. The low-energy dispersion of a (planar) d -wave

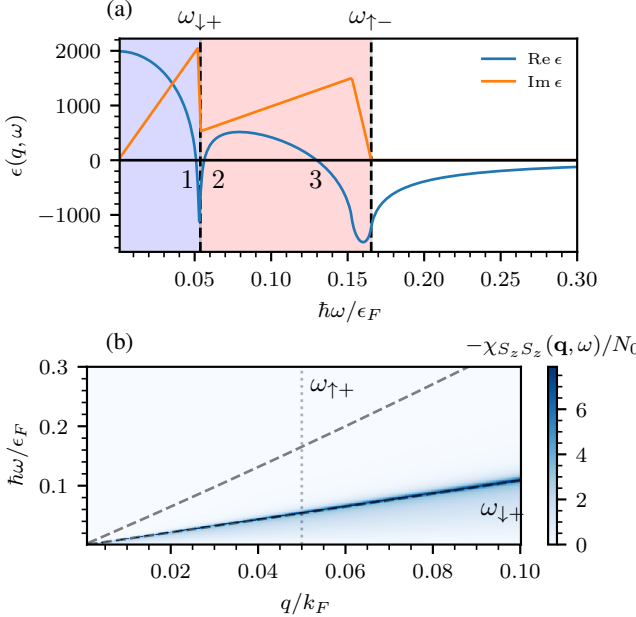


FIG. 2. (a) The real and imaginary part of the dielectric function, for $\mathbf{q}^* = q\hat{\mathbf{x}}$, with $q = 0.05k_F$. The zeros of the real part correspond to resonances, whereas the imaginary part determines their damping. The spin demon is the second zero. The blue and red colors indicate where the spin-down and spin-up particle-hole continuum is non-zero. (b) The spin-density response function, $\text{Im}[\chi_{S_z S_z}(\mathbf{q}, \omega)]$, for $\mathbf{q} \parallel \hat{\mathbf{x}}$, showing the existence of a spin demon with a high quality factor. The vertical dotted line corresponds to the q used in (a). In both (a,b), the dashed lines indicate the edges of the spin-up and spin-down particle-hole continuum, $\omega_{\pm-}$.

altermagnet is then described by [2, 18]

$$\epsilon_{\mathbf{k}}^{\sigma} = \frac{\hbar^2 k^2}{2m_0} + \sigma \frac{\hbar^2 (k_x^2 - k_y^2)}{2m_*}, \quad (2)$$

where we take $m_0 = 0.4m_e$, $m_* = 1.25m_0$ and a Fermi level of $\epsilon_F = 0.5$ eV. Here, m_e is the electron mass. We stress that we assume a closed Fermi surface. The non-interacting density-density response function can then be found analytically from the Lindhard function [19]; we show details in Secs. I and II in the Supplemental Material (SM) [?]. Solving Eq. (1) for $\chi_{\sigma\sigma'}(\mathbf{q}, \omega)$, we find the three response functions $\chi_{nn}(\mathbf{q}, \omega)$, $\chi_{nS_z}(\mathbf{q}, \omega)$, $\chi_{S_z S_z}(\mathbf{q}, \omega)$ [17]. We focus here on $\chi_{S_z S_z}(\mathbf{q}, \omega)$, which shows the strongest signature of the spin demon; we discuss $\chi_{nn}(\mathbf{q}, \omega)$ and $\chi_{nS_z}(\mathbf{q}, \omega)$ in Sec. III in the SM. We thus focus on

$$\chi_{S_z S_z}(\mathbf{q}, \omega) = \frac{\chi_{\uparrow}^{(0)} + \chi_{\downarrow}^{(0)} - 4v_q \chi_{\uparrow}^{(0)} \chi_{\downarrow}^{(0)}}{\epsilon(\mathbf{q}, \omega)} \quad (3)$$

where

$$\epsilon(\mathbf{q}, \omega) \equiv 1 - v_q (\chi_{\uparrow}^{(0)} + \chi_{\downarrow}^{(0)}) \quad (4)$$

is the complex longitudinal dielectric function. Collective modes then emerge as the poles of the response function, de-

termined by the zeroes of the longitudinal dielectric function,

$$\epsilon(\mathbf{q}, \omega) = 0. \quad (5)$$

We first analyze the dielectric function in more detail, by showing $\epsilon(\mathbf{q}, \omega)$ for a fixed $\mathbf{q} \parallel \hat{\mathbf{x}}$ in Fig. 2(a), where we also indicate the spin-polarized particle-hole continua. We observe the existence of three zeros of the dielectric function. The first and third zero correspond to the spin-down and spin-up acoustic plasmon respectively [20], which are overdamped because they live in their respective particle-hole continuum. The second zero however arises because of the interplay of the spin-up and spin-down particles, and corresponds to the spin demon. Importantly, it sits outside of the spin-down continuum, and therefore the imaginary part of the dielectric function is reduced. This implies that the spin demon is potentially underdamped, which we will show in more detail with the imaginary part of the spin-spin response function, $\text{Im}[\chi_{S_z S_z}(\mathbf{q}, \omega)]$ in Fig. 2(b). The sharp resonance close the edge of the spin-down continuum is the spin demon, which we observe to be sharply peaked, although it is not completely undamped, due to a finite overlap with the spin-up continuum. Upon rotation through the altermagnetic spin-split plane, we obtain Fig. 1, demonstrating that the spin demon is most sharply defined along x and y , and vanishes along the nodal lines, where the Fermi surfaces are spin degenerate. The spin demon remains well defined for small tilt angles off the altermagnetic spin split plane, as shown in Sec. IV in the SM.

Analysis. In what follows, we constrain \mathbf{q} to lie in the altermagnetic spin split plane, parametrizing $\mathbf{q} = q(\cos \theta, \sin \theta, 0)$. Our analysis is simplified by defining the projected spin splitting of the particle-hole continuum for spin species σ :

$$\eta_{\sigma}(\theta) \equiv \sqrt{\tilde{m} m_0 \left(1 + \sigma \frac{m_0}{m_*} \cos 2\theta\right)}, \quad (6)$$

where $\tilde{m} \equiv m_0(m_*^2/(m_*^2 - m_0^2))^{1/3}$. We have defined $\eta_{\sigma}(\theta)$ such that $\chi_{\sigma}^{(0)}$ can be obtained from the well-known Lindhard function for spherical Fermi surfaces [17, 21] by rescaling $q \rightarrow \eta_{\sigma}(\theta)q$ and $m \rightarrow \tilde{m}$ [19]. For convenience, we define a spin-independent Fermi wave vector $k_F \equiv \sqrt{2\tilde{m}E_F}/\hbar$ and velocity $v_F \equiv \hbar k_F/\tilde{m}$.

The analysis is simplified by noting that, depending on the angle θ , one of the two spin species can be treated as the (projected) majority spin species, defined such that $\eta_{\text{maj}}(\theta) > \eta_{\text{min}}(\theta)$. For example, along x , spin down is the minority spin species [cf. Fig. 2]. We can then solve for the zero in the dielectric function corresponding to the spin demon by making the ansatz [22]

$$\omega_d(\mathbf{q}) = v_d \eta_{\text{min}}(\theta) q. \quad (7)$$

Additionally, we require the spin demon to have energies in the pseudogap formed by the edges of the spin-resolved particle-hole continua, which are given by $\omega_{\sigma+} = v_F \eta_{\sigma}(\theta) q + O(q^2/k_F^2)$ and indicated in Fig. 2 by dashed lines.

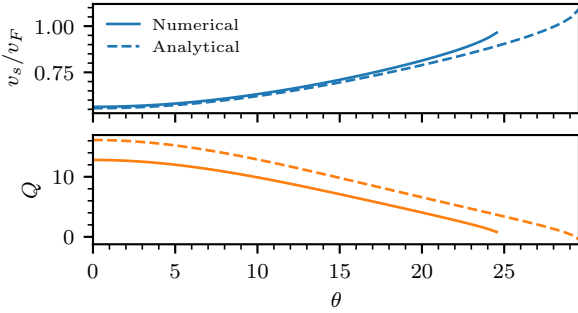


FIG. 3. The spin demon velocity (top) and quality factor (bottom), as a function of the spin demon angle θ . The numerical solutions (solid), are obtained by numerically finding the zeros and corresponding derivatives from the full dielectric function; the analytical solutions (dashed) follow from numerically solving Eq. (8).

We carry out this approach in Sec. VI in the SM, and find that, up to corrections of order $(q/k_F)^2$, the spin demon velocity v_d is determined by

$$4 - \frac{v_d}{v_F} \log \left[\frac{v_F - v_d}{v_d - v_F} \right] - \frac{v_d \eta_{\min}}{v_F \eta_{\maj}} \log \left[\frac{v_F \eta_{\maj} - v_d \eta_{\min}}{v_d \eta_{\min} - v_F \eta_{\maj}} \right] = 0. \quad (8)$$

This has no analytical solutions, and we thus solve it numerically.

In addition to the group velocity of the spin demon, we are also able to obtain the quality factor, defined as $Q \equiv \omega_d/\gamma$, where the damping γ can be obtained by performing a Laurent-Taylor expansion around ω_d to find

$$\gamma = \frac{\text{Im}[\epsilon(\mathbf{q}, \omega)]}{\partial_\omega \text{Re}[\epsilon(\mathbf{q}, \omega)]} \Big|_{\omega=\omega_d}. \quad (9)$$

In Fig. 3, we show v_d and the corresponding quality factor γ as a function of θ . We stress that for quality factors less than unity, the spin demon is no longer a well-defined quasiparticle, which happens for $\theta_c \geq 23^\circ$ for this set of parameters. Up to this critical angle, the velocity of the spin demon only changes by a factor of 2, while the quality factor falls off by one order of magnitude. We note here that the quality factor is not bounded, and increasing the altermagnetic band anisotropy (controlled here by the ratio m_0/m_*) leads to higher quality factors.

Out-of-phase oscillations and magnetic moment. To gain more insight in the character of the spin demon, we solve the eigenvalue problem defined by Eq. (1),

$$\begin{pmatrix} \text{Re}[\chi_\uparrow^{(0)}(\omega)]^{-1} - v_q & -v_q \\ -v_q & \text{Re}[\chi_\uparrow^{(0)}(\omega)]^{-1} - v_q \end{pmatrix} \begin{pmatrix} \psi_\uparrow \\ \psi_\downarrow \end{pmatrix} = 0, \quad (10)$$

which has the solution

$$\frac{\psi_{\maj}}{\psi_{\min}} = -\frac{v_q N_0}{1 + v_q N_0} \approx -1 + O(q^2/k_F^2), \quad (11)$$

where $N_0 = \tilde{m}k_F/(2\pi^2\hbar^2)$ is the spin-independent density of states at the Fermi level. This result thus clearly shows that in the limit of small q/k_F , the spin demon consists of out-of-phase oscillations of two spin-species—in contrast to the conventional plasmon, which consist of in-phase oscillations. In addition, Eq. (11) shows that as q/k_F approaches zero, $|\psi_{\maj}| < |\psi_{\min}|$. We therefore expect that a spin demon carries a magnetic moment, since it is composed of predominantly one spin species.

To show this in more detail, we consider an external magnetic field B , which is orientated along the Néel vector. The electrons then gain energy $\sigma g_e \mu_B B$, where $g_e \approx 2$ is the electron gyromagnetic ratio and μ_B is the Bohr magneton. We furthermore assume the magnetic field to not affect the magnetic texture, which would be the case in the presence of a (weak) easy-axis anisotropy, and we neglect orbital magnetization effects. We now calculate the magnetic moment, which is defined as

$$\mu_d \equiv -\hbar \frac{\partial \omega_d}{\partial B}, \quad (12)$$

In the limit of $\eta_{\min}(\theta)/\eta_{\maj}(\theta) \rightarrow 0$ we have

$$\frac{\partial v_d}{\partial B} = v'_d \frac{\partial \Delta}{\partial B} + O(\Delta^2), \quad (13)$$

where $\Delta \equiv g_e \mu_B B N'_0 / N_0$, $v'_d = 8e^{-4}v_F$ and $N'_0 = \partial N_0(\epsilon)/\partial \epsilon|_{\epsilon=\epsilon_F}$. This allows us to obtain the magnetic moment as

$$\mu_d = g_e \mu_B \hbar \frac{N'_0}{N_0} \eta_{\min}(\theta) v'_d q. \quad (14)$$

Importantly, Eq. (14) implies that a spin demon can carry angular momentum. In addition, since the minority spin species switches between spin-up and spin-down as the spin demon is rotated through the plane, the magnetic moment has the opposite sign for $\mathbf{q} \parallel \hat{\mathbf{y}}$, representing the d -wave symmetry of the underlying altermagnetic band structure.

We show this in more detail in Fig. 4, where we have numerically calculated the magnetic moment of the spin demon as a function of θ . For the angles where the spin-up species is the majority species, we obtain a positive magnetic moment, whereas for the angles where the spin-down species is dominant, we have a negative magnetic moment. The magnetic moment thus captures the d -wave symmetry of the underlying altermagnetic band structure. The size of the magnetic moment is also shown, where we remind the reader that it is proportional to q [see Eq. (14)]. For $q = 0.05k_F$, we obtain that $\mu_p \approx 0.025\mu_B$ for $\mathbf{q} \parallel \hat{\mathbf{x}}$. The magnetic moments grows to $0.1\mu_B$ for angles approaching the critical angle—but the quality factor also decreases, such that these magnetic moments might not be observable.

These results show that an applied magnetic field will shift the spin demon frequencies up or down, depending on the orientation of \mathbf{q} . The absolute shift in the spin demon frequency is however small, approximately $1.5\mu\text{eV}$ at $\mathbf{q} = 0.05k_F \hat{\mathbf{x}}$ with

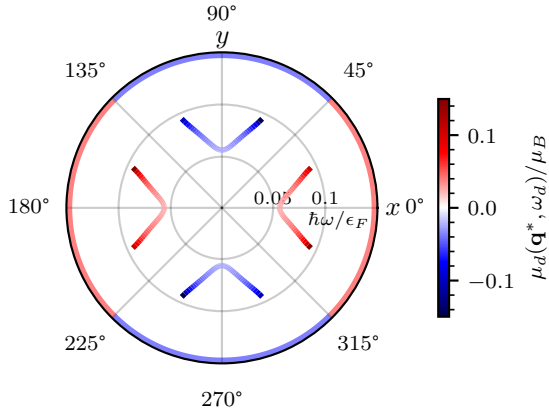


FIG. 4. The numerically obtained spin demon resonance frequency ω_d as a function of $\mathbf{q}^* = q(\cos \theta, \sin \theta, 0)$, with $q = 0.05k_F$, rotated in the altermagnetic spin splitting plane with angle θ . The color corresponds to the magnetic moment, showing the d -wave character. The numerical solutions are obtained by numerically finding the zeros and evaluating Eq. (12) from the full dielectric function. Along x and y , the magnetic moment is approximately $\pm 0.025\mu_B$. The colors on the ring indicate the projected spin species, with red (blue) spin up (down).

a magnetic field of 1 T, whereas the energy of the spin demon is 2.8 meV, resulting in a relative shift of 0.1%. Alternatively, all that is required is a sublattice-sensitive experimental handle, for example achievable through piezomagnetism [5].

Two-dimensional. The spin demon as considered here also exists in two-dimensional altermagnets. The analysis in 2D is similar to in 3D, and we relegate details to Sec. VII in the SM. We choose the same parameters as in 3D.

We show the resulting spin-spin response function in Fig. 5, highlighting the same four-fold rotational symmetry. In addition, we show the spin demon velocity and quality factor as a function of the projected spin splitting in 2D. Because the particle-hole continuum is sharply defined in two dimensions, we are able to provide analytical solutions of the spin demon velocity and quality factor as [14]

$$v_d^{2D} = \frac{2}{\sqrt{3}} v_F \eta_{\min}(\theta) q + O(q^2/k_F^2) \quad (15)$$

$$Q^{2D} = \frac{3 \sqrt{4\eta_{\min}^2(\theta) - 3\eta_{\text{maj}}^2(\theta)}}{\eta_{\min}(\theta)} + O(q^2/k_F^2), \quad (16)$$

for $2\eta_{\min}(\theta) > \sqrt{3}\eta_{\text{maj}}(\theta)$, whereas the spin demon ceases to exist if this condition is not met.

We observe that the spin demon in two dimensions is more robust than in 3D, surviving for larger θ (39.9° versus $\approx 23^\circ$). We stress that spin demon ceases to exist for $\theta \geq 39.9^\circ$, and beyond this angle we observe the remnants of the overdamped conventional acoustic plasmon. The quality factors are however comparable in magnitude, especially for angles that align with the altermagnetic axis. Finally, we comment that in 2D, the spin demon also has a magnetic moment (shown in Sec. VII in the SM), which is comparable in magnitude to the

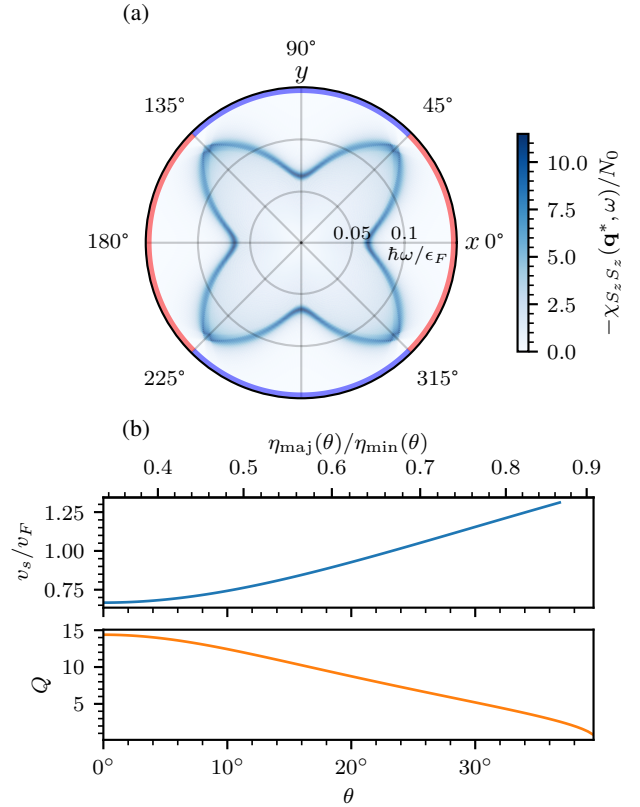


FIG. 5. In two dimensions: (a) $\text{Im}[\chi_{S_zS_z}(\mathbf{q}^*, \omega)]$, The angle indicates θ and the radial axis the frequency ω . (b) The spin demon velocity (top) and quality factor (bottom) as a function of rotation angle θ .

3D case and displays the same altermagnetic symmetry.

Conclusion. We have shown that both three and two dimensional altermagnetic metals can host out-of-phase oscillations of the two spin densities, thus realizing a spin demon. The spin demon has a magnetic moment, which has opposite sign for propagation along different angles through the altermagnetic plane, inheriting the d -wave symmetry of the altermagnet.

We have considered here only the RPA, which we expect to provide a fair description, since corrections to the RPA have been shown to mainly only enhance the damping of comparable acoustic plasmons in a two-dimensional spin-polarized electron gas [23]. We expect the same conclusions to hold for spin demons in altermagnetic metals.

In this work, we have considered a d -wave altermagnet, where the spin-split Fermi surfaces are elliptical. We have repeated the same analysis for a g -wave altermagnet in Sec. VIII in the SM, where we find that the separation of the spin-polarized particle-hole continua is not sufficient for a spin demon to emerge. We therefore conclude that the spin demon is a specific feature of d -wave altermagnets.

The spin demon could be directly observed by making use of spin-sensitive electron scattering probes, such as spin-polarized electron energy loss spectroscopy (SPEELS) [24] or

cross-polarized Raman scattering [25]. These probes directly measure $\text{Im}[\chi_{S_z S_z}(\mathbf{q}, \omega)]$ (or $\text{Im}[\chi_{n S_z}(\mathbf{q}, \omega)]$, which also contains information of the spin demon; see Sec. III in the SM), and can thus map Fig. 1 and Fig. 2(a).

Real samples will most likely consist of multiple magnetic domains with different orientations of the Néel vector. We expect that this will not be a difficulty for the detection of the spin demon, since typical domain sizes in altermagnets can be in the micrometer range [26], placing an upper limit on the spin demon wavelength of micrometers. A probe which is spatially localized on this length scale can then directly detect spin demons. In addition, recent transport experiments have measured a finite anomalous Hall effect signal, demonstrating that altermagnetic domains are not equally populated [27–29], and thus even a spatially delocalized probe could detect spin demons.

* pgunnink@uni-mainz.de

- [1] L. Šmejkal, J. Sinova, and T. Jungwirth, Beyond Conventional Ferromagnetism and Antiferromagnetism: A Phase with Non-relativistic Spin and Crystal Rotation Symmetry, *Physical Review X* **12**, 031042 (2022).
- [2] L. Šmejkal, J. Sinova, and T. Jungwirth, Emerging Research Landscape of Altermagnetism, *Physical Review X* **12**, 040501 (2022).
- [3] R. Zarzuela, R. Jaeschke-Ubiergo, O. Gomonay, L. Šmejkal, and J. Sinova, *Transport theory and spin-transfer physics in d-wave altermagnets* (2024), arXiv:2412.13763 [cond-mat].
- [4] C.-T. Liao, Y.-C. Wang, Y.-C. Tien, S.-Y. Huang, and D. Qu, Separation of Inverse Altermagnetic Spin-Splitting Effect from Inverse Spin Hall Effect in RuO₂, *Physical Review Letters* **133**, 056701 (2024).
- [5] T. Aoyama and K. Ohgushi, Piezomagnetic properties in altermagnetic MnTe, *Physical Review Materials* **8**, L041402 (2024).
- [6] K. V. Yershov, V. P. Kravchuk, M. Daghofer, and J. van den Brink, Fluctuation-induced piezomagnetism in local moment altermagnets, *Physical Review B* **110**, 144421 (2024).
- [7] S. Karube, T. Tanaka, D. Sugawara, N. Kadoguchi, M. Kohda, and J. Nitta, Observation of Spin-Splitter Torque in Collinear Antiferromagnetic \$\{\text{RuO}_2\}\$, *Physical Review Letters* **129**, 137201 (2022).
- [8] Z. Liu, M. Ozeki, S. Asai, S. Itoh, and T. Masuda, Chiral Split Magnon in Altermagnetic MnTe, *Physical Review Letters* **133**, 156702 (2024).
- [9] L. Šmejkal, A. Marmodoro, K.-H. Ahn, R. González-Hernández, I. Turek, S. Mankovsky, H. Ebert, S. W. D’Souza, O. Šípr, J. Sinova, and T. Jungwirth, Chiral Magnons in Altermagnetic RuO₂, *Physical Review Letters* **131**, 256703 (2023).
- [10] D. Pines, Electron interaction in solids, *Canadian Journal of Physics* **34**, 1379 (1956).
- [11] J. Ruvalds, Are there acoustic plasmons?, *Advances in Physics* **30**, 677 (1981).
- [12] S. Das Sarma and A. Madhukar, Collective modes of spatially separated, two-component, two-dimensional plasma in solids, *Physical Review B* **23**, 805 (1981).
- [13] R. Sensarma, E. H. Hwang, and S. Das Sarma, Dynamic screening and low-energy collective modes in bilayer graphene, *Physical Review B* **82**, 195428 (2010).
- [14] A. Agarwal, M. Polini, G. Vignale, and M. E. Flatté, Long-lived spin plasmons in a spin-polarized two-dimensional electron gas, *Physical Review B* **90**, 155409 (2014).
- [15] K. Sadhukhan, A. Politano, and A. Agarwal, Novel Undamped Gapless Plasmon Mode in a Tilted Type-II Dirac Semimetal, *Physical Review Letters* **124**, 046803 (2020).
- [16] A. A. Husain, E. W. Huang, M. Mitrano, M. S. Rak, S. I. Rubeck, X. Guo, H. Yang, C. Sow, Y. Maeno, B. Uchoa, T. C. Chiang, P. E. Batson, P. W. Phillips, and P. Abbamonte, Pines’ demon observed as a 3D acoustic plasmon in Sr₂RuO₄, *Nature* **621**, 66 (2023).
- [17] G. Giuliani and G. Vignale, *Quantum Theory of the Electron Liquid* (Cambridge University Press, 2005).
- [18] M. Roig, A. Kreisel, Y. Yu, B. M. Andersen, and D. F. Agterberg, Minimal models for altermagnetism, *Physical Review B* **110**, 144412 (2024).
- [19] S. Ahn and S. Das Sarma, Anisotropic fermionic quasiparticles, *Physical Review B* **103**, 045303 (2021).
- [20] A. Kamenev, *Field Theory of Non-Equilibrium Systems*, 2nd ed. (Cambridge University Press, 2023).
- [21] J. Lindhard, On the properties of a gas of charged particles, *Kgl. Danske Videnskab. Selskab Mat.-fys. Medd.* **28**, No. 8 (1954).
- [22] G. E. Santoro and G. F. Giuliani, Acoustic plasmons in a conducting double layer, *Physical Review B* **37**, 937 (1988).
- [23] D. Kreil, R. Hobbiger, J. T. Drachta, and H. M. Böhm, Excitations in a spin-polarized two-dimensional electron gas, *Physical Review B* **92**, 205426 (2015).
- [24] M. Plihal, D. L. Mills, and J. Kirschner, Spin Wave Signature in the Spin Polarized Electron Energy Loss Spectrum of Ultrathin Fe Films: Theory and Experiment, *Physical Review Letters* **82**, 2579 (1999).
- [25] J. Kim, J.-U. Lee, and H. Cheong, Polarized Raman spectroscopy for studying two-dimensional materials, *Journal of Physics: Condensed Matter* **32**, 343001 (2020).
- [26] O. J. Amin, A. Dal Din, E. Golias, Y. Niu, A. Zakharov, S. C. Fromage, C. J. B. Fields, S. L. Heywood, R. B. Cousins, F. Maccherozzi, J. Krempaský, J. H. Dil, D. Kriegner, B. Kiraly, R. P. Campion, A. W. Rushforth, K. W. Edmonds, S. S. Dhesi, L. Šmejkal, T. Jungwirth, and P. Wadley, Nanoscale imaging and control of altermagnetism in MnTe, *Nature* **636**, 348 (2024).
- [27] S. G. Jeong, S. Lee, B. Lin, Z. Yang, I. H. Choi, J. Y. Oh, S. Song, S. wook Lee, S. Nair, R. Choudhary, J. Parikh, S. Park, W. S. Choi, J. S. Lee, J. M. LeBeau, T. Low, and B. Jalani, *Metallicity and Anomalous Hall Effect in Epitaxially-Strained, Atomically-thin RuO₂ Films* (2025), arXiv:2501.11204 [cond-mat].
- [28] M. Leiviskä, J. Rial, A. Bad’ura, R. L. Seeger, I. Kounta, S. Beckert, D. Kriegner, I. Joumard, E. Schmoranzerová, J. Sinova, O. Gomonay, A. Thomas, S. T. B. Goennenwein, H. Reichlová, L. Šmejkal, L. Michez, T. Jungwirth, and V. Baltz, Anisotropy of the anomalous Hall effect in thin films of the altermagnet candidate Mn₅Si₃, *Physical Review B* **109**, 224430 (2024).
- [29] H. Reichlova, R. Lopes Seeger, R. González-Hernández, I. Kounta, R. Schlitz, D. Kriegner, P. Ritzinger, M. Lammel, M. Leiviskä, A. Birk Hellenes, K. Olejník, V. Petříček, P. Doležal, L. Horak, E. Schmoranzerova, A. Badura, S. Bertaina, A. Thomas, V. Baltz, L. Michez, J. Sinova, S. T. B. Goennenwein, T. Jungwirth, and L. Šmejkal, Observation of a spontaneous anomalous Hall response in the Mn₅Si₃ d-wave altermagnet candidate, *Nature Communications* **15**, 4961 (2024).